Wang *et al. Carbon Footprints* 2024;3:14
DOI: 10.20517/cf.2024.19

Carbon Footprints

Original Article

Open Access

Open-data-based city-scale gridded carbon dioxide emission inventory: supporting urban carbon monitoring in Chengdu, China

Rui Wang[1,2], Yuzhong Zhang[1,2], Shuang Zhao[1,2], Xinlu Wang[1,2,3]

[1]Key Laboratory of Coastal Environment and Resources of Zhejiang Province, School of Engineering, Westlake University, Hangzhou 310030, Zhejiang, China.
[2]Institute of Advanced Technology, Westlake Institute for Advanced Study, Hangzhou 310024, Zhejiang, China.
[3]College of Environmental and Resource Sciences, Zhejiang University, Hangzhou 310058, Zhejiang, China.

Correspondence to: Prof. Yuzhong Zhang, Key Laboratory of Coastal Environment and Resources of Zhejiang Province, School of Engineering, Westlake University, No. 600 Dunyu Road, Hangzhou 310030, Zhejiang, China. E-mail: zhangyuzhong@westlake.edu.cn

How to cite this article: Wang R, Zhang Y, Zhao S, Wang X. Open-data-based city-scale gridded carbon dioxide emission inventory: supporting urban carbon monitoring in Chengdu, China. *Carbon Footprints* 2024;3:14. https://dx.doi.org/10.20517/cf.2024.19

Received: 27 Jun 2024 **First Decision:** 24 Aug 2024 **Revised:** 5 Sep 2024 **Accepted:** 10 Sep 2024 **Published:** 21 Sep 2024

Academic Editors: Hui Wang, Yuli Shan **Copy Editor:** Fangling Lan **Production Editor:** Fangling Lan

Abstract

Gridded carbon dioxide (CO_2) emission inventories are usually required as prior information for deriving urban-scale emissions from atmospheric CO_2 monitoring data. However, existing global or national gridded inventories are inadequate for this purpose because of their failure to accurately resolve the spatial distribution of urban emissions, especially from point sources, at the city scale. To address this challenge, we developed a city-scale gridded CO_2 emission inventory mode that spatially disaggregated sectorial CO_2 emissions of a city to a high-resolution grid. We compiled a series of sector-specific, high-resolution proxies for spatial disaggregation by integrating multiple open data, including remote sensing imagery and urban big data. As a demonstration, we applied the methodology to Chengdu, China, for a gridded CO_2 emission inventory at a 1 km resolution for 2020. This inventory offered a clear and comprehensive depiction of the spatial distribution of CO_2 emissions at the city scale, identified high-emission areas, and delivered essential scientific support and decision-making tools for effective carbon management. For example, compared to global or national inventories (e.g., EDGAR) that use population or GDP as proxy data for industrial emissions, this inventory provided more accurate locations of industrial point source emissions by including information on 50,000 industrial sources collected from open sources. The improved spatial distribution of the gridded inventory allows for more accurate and reliable flux inversion, establishing a robust data foundation for the development of CO_2 concentration monitoring networks.

Keywords: Carbon dioxide, gridded emission inventory, city scale, city big data, carbon monitoring, spatial allocation

INTRODUCTION

Global carbon dioxide (CO_2) emissions have been rising at an alarming rate, driven primarily by fossil fuel consumption, industrial activities, and deforestation. These emissions contributed to global warming and resulting climate change, which posed a severe threat to ecosystems, economies, and human health worldwide[1]. Despite international society's efforts to curb CO_2 emissions, including agreements such as the Paris Agreement[2], global emissions continued to increase, with significant contributions from both developed and developing nations, emphasizing the need for immediate and sustained reductions in global CO_2 emissions to mitigate the worst impacts of climate change[3,4]. In response, many countries were implementing ambitious policies and initiatives, such as transitioning to renewable energy sources, enhancing energy efficiency, promoting electric vehicles[5], and investing in carbon capture and storage technologies[6]. These measures are critical to meeting global climate targets and slowing the pace of climate change.

In this global context, China pledged in 2020 to strive for carbon peaking by 2030 and achieve carbon neutrality by 2060 in response to the escalating global warming crisis and the imperative to mitigate CO_2 emissions[7,8]. This commitment reflects China's active engagement in addressing climate change and underscores its dedication to sustainable development and environmental protection. As the world's largest CO_2 emitter, driven by rapid urbanization and industrialization, China recognizes the critical importance of developing city-specific emission reduction policies[9]. In alignment with this goal, the Ministry of Ecology and Environment of the People's Republic of China launched the "Pilot Project for Carbon Monitoring and Assessment" in September 2021. This project aimed to implement pilot projects focusing on carbon monitoring and assessment in target cities and key industries to enhance the collaborative monitoring capability of pollution and carbon reduction. Chengdu, one of the 16 pilot cities, would concentrate on high-resolution and high-precision CO_2 monitoring and assessment, establishing a comprehensive CO_2 concentration monitoring network.

Recognizing the central role of cities in achieving these ambitious goals, China's carbon emission mitigation initiatives have focused on city areas, which were crucial participants in the realization of CO_2 emissions control objectives[10-12]. As primary hubs for human activities, cities concentrate substantial population, exhibit high economic density, and display elevated energy consumption intensity, thereby emerging as a significant source of anthropogenic CO_2 emissions[13]. From a global perspective, according to statistical analyses, Wei *et al.* (2021) stated that among the 167 cities or metropolitan areas across 53 countries, the top 25 cities alone contributed to more than half of the global emissions[14]. Another survey from the International Energy Agency (IEA) estimated that city areas accounted for 71% of global energy consumption CO_2 emissions[15]. In China, where rapid urbanization continued to drive population migration to cities, 40% of city residents consumed 75% of the total energy[16], leading to city environmental degradation, particularly in the thermal environment, due to increased fuel usage, material consumption, housing demand, and uncontrolled land use expansion[17-20]. Owing to their substantial energy consumption driven by construction, production, and economic growth, cities have become critical arenas for implementing emission-reduction strategies and are central to the global search for climate change mitigation solutions[21-24].

To establish city-scale carbon monitoring networks that can effectively guide regional CO_2 emission reduction, CO_2 emission flux inversion is essential. This inversion process not only helps identify specific emission sources but also provides key data for policymakers to implement effective emission reduction

strategies at the city scale. CO_2 emission flux inversion relies on gridded emission inventories as prior information. These inventories provide the spatial resolution required to relate emissions to atmospheric concentrations using atmospheric transport models[9,25]. Large errors in the spatial distribution and sectoral categorization of these prior inventories would cause significant biases in the posterior estimates, which can further mislead the interpretation of the posterior results. Therefore, a gridded emission inventory that represents our best knowledge of the spatial distribution is required for successfully deriving city-scale carbon emissions from a carbon monitoring network.

The Emission Database for Global Atmospheric Research (EDGAR) global emission inventory is often used as prior information due to its unique comprehensive global inventory, detailed spatial information at a fine resolution of 0.1° × 0.1°, and extensive data on greenhouse gas (GHG) emissions from energy production, industrial processes, waste disposal, and biomass burning since 1970[26-28]. These high-resolution data are important for accurately representing the spatial distribution of emissions in global atmospheric models and inversion studies[29]. However, several studies have demonstrated that EDGAR inventory, due to its biases in spatial information and emission estimates, could introduce substantial errors into posterior results when used as prior information. Hu *et al.* (2022) highlighted that the accuracy of power plant locations in the prior information has a substantial impact on the estimated city CO_2 emissions flux in the study on CO_2 emissions in Nanchang, Jiangxi Province, China[30]. Maasakkers *et al.* (2019) discussed the impact of using EDGAR v4.3.2 inventory as prior emission inventories on inversion results of methane emissions using Greenhouse gases observing satellite (GOSAT) data[31]. Their study highlighted the discrepancies between prior inventory results, particularly noting the overestimation of methane emissions in certain regions, especially in China (coal emissions) and in the Middle East (oil and gas emissions)[31]. Lyon *et al.* (2015) demonstrated that the methane emission inventory constructed in that study for the Barnett Shale region exhibited significantly higher accuracy and detail compared to the EDGAR inventory[32]. Further, the low resolution of such inventories failed to capture the intricate pattern of CO_2 emissions in city areas, leading to significant uncertainties in spatial distribution at the city scale[33,34]. Large-scale inventories, such as EDGAR inventory, typically use national emission factors and activity data. However, they often lack essential spatial information and rely instead on proxy data, such as GDP or population data, to represent emission distribution. This approach could result in significant discrepancies in capturing the actual spatial variability of emissions within cities. Compared to large-scale, low-resolution inventories, previous studies about high-resolution emission inventories tailored for city-scale or region-scale also had shortcomings. High spatial resolution is a key factor influencing the accuracy of emission inversion results[35]. Utilizing high-resolution proxy data for the direct spatial allocation of emissions is a common practice for the compilation of gridded emission inventories. However, most existing studies on gridded emission inventories have not comprehensively compiled emissions across all sectors, often focusing on key sectors such as industrial point sources and transportation sources[36-38] for GHG or air pollutant emissions. Additionally, several studies have relied on relatively homogeneous proxy data, primarily including nighttime light data, population distribution, or GDP distribution[39,40]. This limitation has hindered the use of the most appropriate proxy data for spatial allocation for each sector, thereby increasing the uncertainty of gridded emission inventories.

To address the shortcomings of existing inventories, this study focused on the development of a comprehensive, multi-sector gridded CO_2 emission inventory for Chengdu at a 1 km resolution based on multiple open data sources. By integrating diverse proxy data with spatial allocation algorithms, this research offered a more refined description of spatial distribution characteristics of city CO_2 emissions and provided a robust data foundation for city-scale carbon flux inversions. Moreover, this study contributed to the broader discourse on carbon management by highlighting the importance of high-resolution emission inventories in supporting local and regional climate policies.

MATERIAL AND METHODS

Study area

Chengdu, the capital of Sichuan Province in southwestern China [Figure 1], is strategically located in the fertile Chengdu Plain, surrounded by mountains. With a population of over 20 million, it ranks among China's largest and most vibrant cities. While renowned for its advanced high-tech industries, Chengdu also hosts some high-emission sectors, such as cement manufacturing. Its extensive road network enhances regional connectivity and logistics but also contributes to significant traffic-related carbon emissions.

Data sources and data collection

As the foundation of this research, the data collection and screening process was particularly indispensable. To ensure the smooth progress of subsequent research, data collection was divided into two parts: tabular CO_2 emission inventory and spatial proxy data. Additionally, only publicly available data were collected to facilitate the future dissemination and application of this methodology. Figure 2 illustrates the datasets required for this study, along with the corresponding spatial proxy data used for the spatial allocation of emission quantities across various sectors.

The tabular CO_2 emission inventory was sourced from the "China City Carbon Dioxide Emission Dataset (CCCED)"[41], which provides CO_2 emissions from various sectors, including agriculture, services, industry, residential, and transportation. We selected appropriate spatial proxy data that match the characteristics of each sector for emission allocation. Detailed corresponding proxy data of each sector are listed in Table 1. Due to the lack of a distinct classification of industrial energy and industrial processing, the emissions for individual industry sectors could not be represented accurately, resulting in significant uncertainty in point source emissions. Consequently, it was necessary to reclassify the emission sectors. Detailed emission data processing and reclassification can be found in Supplementary Material Section 1. After reclassification, CO_2 emissions by each sector area are shown in Figure 3, where dashed circular arcs represent point source emissions, and solid circular arcs indicate non-point sources. According to CCCED, the total CO_2 emissions of Chengdu in 2020 were 4.277 million tons. The transportation sector was the largest contributor, with emissions reaching 15.47 million tons, representing 36.2% of the total emissions. Due to the electrification transition of China's railways transportation, emissions could be considered negligible. Air transportation emissions were estimated based on aviation fuel consumption; however, this method could not account for the fuel consumption for flights within Chengdu's jurisdiction. Therefore, this study did not analyze air transportation emissions. The second and third largest emission sources were the industrial energy and industrial processing sectors, with emissions of 11.82 and 8.22 million tons, respectively, accounting for 27.6% and 19.2% of the total emissions.

The selection of proxy data was influenced by the ease of data acquisition, the correlation between the proxy data and the emission sources, and the accuracy of the proxy data. The proxy data for point source emissions mainly included latitude and longitude coordinates and emission scale of emitting enterprises and service points of interest (POI). For non-point source emissions, the data included population distribution, land cover, and road networks.

As the proxy data of point sources, the location information of the enterprises and service POI were obtained from the API interface of the online map platform. Industrial point sources, as the major emission sources, included a total of 49,350 industrial POIs from the online map platform. These data contained three key attributes: name, type, and geographic coordinates. Subsequently, the registration information for

Table 1. CO_2 emission source classification and the proxy data for spatial allocation

CO_2 emission source		Emission type	Proxy data
Category	**Type**		
Industry	Industrial energy	Point sources	Latitude and longitude coordinates of emitting enterprise and service POI, enterprise size, *etc.*
	Industrial processing		
Service	-		
Residential	-	Non-point sources	Population distribution data
Agriculture	-		Land cover data
Transportation	Road transportion		Traffic network and rated traffic volume at all road levels
	Waterborne transportion		Water distribution and ship routes

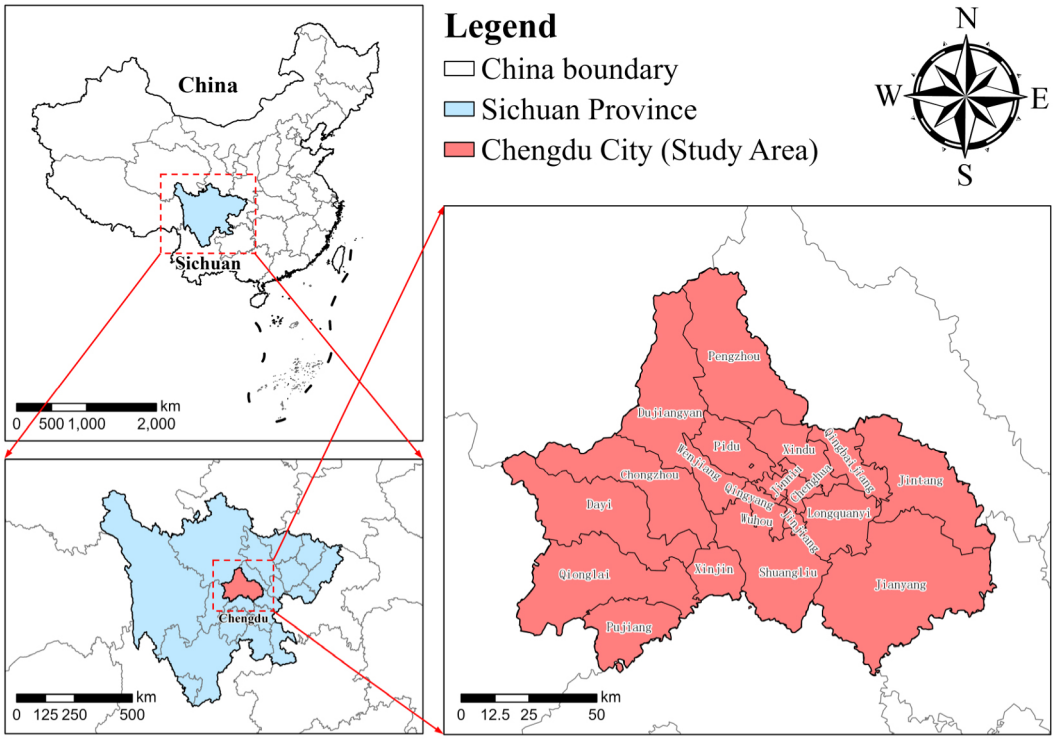

Figure 1. Geographical location of Chengdu city as a study area in China.

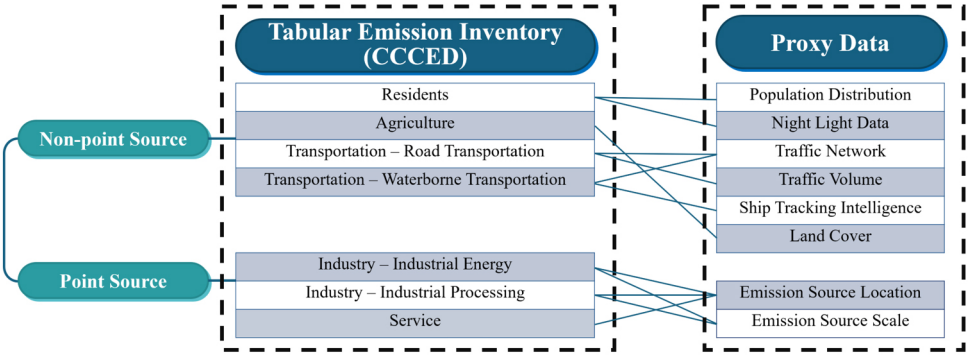

Figure 2. Correspondence between emission sectors and proxy data.

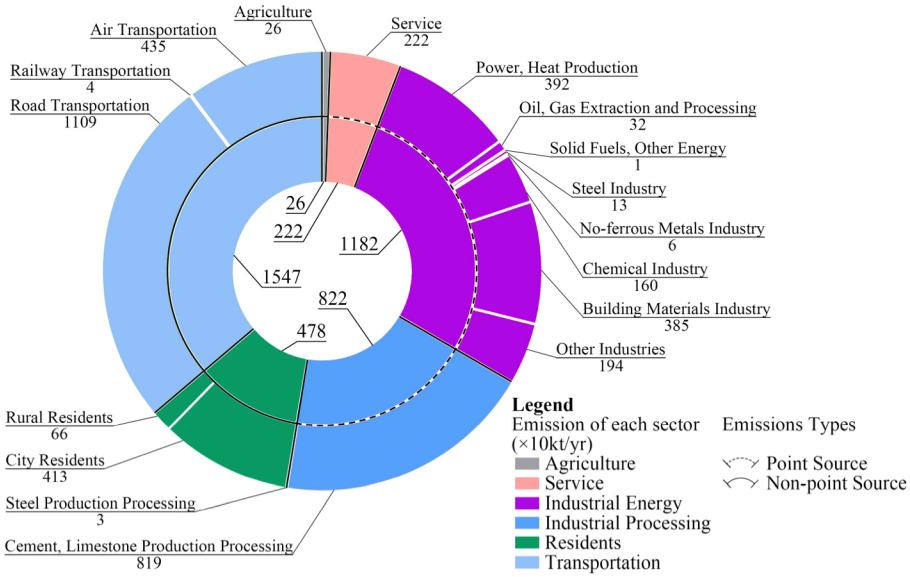

Figure 3. Reclassified CO_2 emissions by sectors, including 6 categories and 17 types.

these POIs was retrieved from TianYanCha[42], an enterprise information query platform. The detailed retrieval process is shown in Supplementary Material Section 2. A total of 5,335 emission point sources from relevant enterprises were obtained by screening the business scope of the enterprises.

The proxy data required for the spatial allocation of non-point source emissions [Table 2] encompassed population counts, nighttime light data, road networks, road traffic volume, waterways, ship tracking intelligence, and land cover. Population counts were downloaded from WorldPop Hub[43] with a spatial resolution of 100 m. Nighttime light data were obtained from VIIRS Nighttime Light[44]. The road networks and waterways obtained from OpenStreetMap (OSM)[45] were used to calculate "road density" and "waterways density". Road traffic volume, obtained according to standards[46,47], was applied to calculate traffic density within each grid. Waterways supplemented with ship tracking intelligence[48] could identify the shipping routes accurately. Land cover data utilized for the spatial allocation of agricultural emissions were sourced from NASA MODIS production[49]. The detailed proxy data are shown in Supplementary Material Section 3.

Spatial allocation

The spatial allocation of CO_2 was based on the ArcGIS platform. Firstly, grids with a spatial resolution of 1 km were established over the study area. This resolution was selected to balance detail and computational efficiency, providing sufficient spatial accuracy to describe the heterogeneity in emissions while remaining manageable in terms of computational load. Observations from satellite imagery further supported this choice, confirming that the top 500 point sources, which account for 89.59% of total emissions, predominantly occupied areas smaller than 1 km^2, with only a few extremely high-emission sources exceeding this size. Then, the data extraction function of ArcGIS was used to extract proxy data including population, road network, latitude and longitude of emission enterprises. Subsequently, the data statistics and management functions of ArcGIS were applied to allocate the emission from several sectors to the corresponding target grids in the following ways. By implementing these detailed procedures, we ensured a precise and systematic allocation of CO_2 across the study area, enhancing the accuracy and reliability of the grided emission inventory.

Table 2. The proxy data and related data used in this study and their sources.

Data	Name	Data source	Description
Population counts	chn_ppp_2020	WorldPop Hub[43]	GeoTIFF, 100 m
Nighttime light data	VNL_v2_npp_2020	VIIRS Nighttime Light[44]	GeoTIFF, 15 arc second (~500 m at the Equator)
Road networks	osm_roads	OpenStreetMap[45]	Shapefile
Road traffic volume	-	Code for Design of Urban Road Engineering[46] Technical Standard of Highway Engineering[47]	Average daily traffic for roads at all levels
Waterways	osm_waterways	OpenStreetMap[45]	Shapefile
Ship tracking intelligence	-	MarineTraffic[48]	Global ship real-time position information
Land cover	MCD12Q1.A2020	NASA MODIS production[49]	Hierarchical data format 4 file, 500 m

(1) Spatial allocation of point source emissions

For point source emissions, the spatial allocation process involved several key steps, as shown in Figure 4A. Latitude and longitude information was directly used to pinpoint the location of the emission source and allocate the emissions to the corresponding target grids. However, during the spatial allocation process, challenges arose with several large industrial facilities that occupy extensive areas, which made it difficult to accurately allocate specific emission points. Therefore, further processing was required for such emissions from large-scale and broad-footprint factories. To address this, the top 500 point sources mentioned above were manually screened to ensure accurate location identification for high-emission sources.

Given that most large enterprises had multiple emission sources, it was complex to determine the exact location of each emission source. Therefore, it was assumed that emissions were uniformly distributed within the factory area. Based on this assumption, for factories spanning multiple grids, the process began with identifying point source locations on the map using latitude and longitude coordinates, followed by delineating enterprise boundaries with satellite imagery, as shown in Step 1 in Figure 4A. Then, spatial data overlay analysis was used to disaggregate the enterprise across the corresponding grids, determining the location and quantity of grids in which the enterprise was located. Finally, emissions were evenly allocated across these intersecting grids, as shown in Step 2 in Figure 4A. If there were multiple point sources within a single grid, their emissions would be summed up. This method effectively solved the problem of spatial allocation posed by multiple point sources in large enterprises, ensuring the accurate distribution of emissions to target grids.

(2) Spatial allocation of non-point source emissions

Non-point source emissions were allocated using spatial proxy data, including population distribution, road traffic density, and agricultural land distribution as weight factors. To ensure effective spatial allocation of these emissions, the proxy data needed to be preprocessed.

For instance, this study focused on preprocessing population distribution data, which served as a proxy for resident emissions. The WorldPop population data was utilized initially; however, it displayed noticeable inconsistencies, particularly in city centers, where the data showed jagged distribution patterns that did not accurately reflect the actual population distribution. To address this issue, nighttime light data, which could partially reflect population distribution, was employed as a correction variable. The preprocessing involved setting the population data as the dependent variable and nighttime light data as the independent variable. A random forest model was then applied to fit these variables and develop an appropriate model for correction. The random forest model yielded a coefficient of determination (R^2) of 0.8665, indicating a

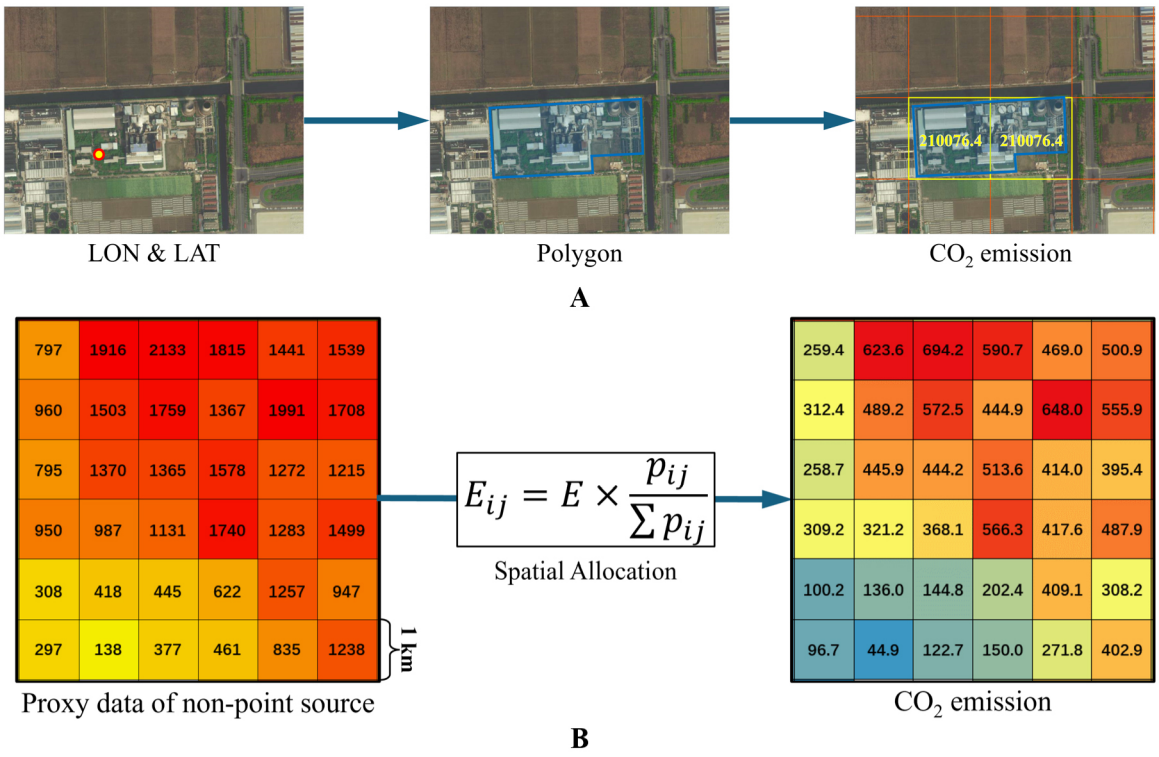

Figure 4. The spatial allocation methods of point source (A) and non-point source (B) CO_2 emission.

strong correlation between the population distribution and nighttime light data. Using this model, the population distribution data were corrected and refined to more accurately represent resident emissions. Further detailed preprocessing of non-point source emissions for various sectors is provided in Supplementary Material Section 4.

These proxy data were used to proportionally allocate emissions to the target grids by assigning emission values based on the relative densities indicated by each proxy. The spatial allocation method for non-point sources is illustrated in Figure 4B. For instance, areas with higher population density, road traffic density, or agricultural activity were allocated higher emission values compared to areas with lower densities. This approach ensured that emissions were distributed in a manner that reflected the underlying spatial characteristics of each proxy data type. Consequently, the emissions were accurately apportioned across the grid cells, aligning with the distribution patterns of the proxy data and providing a more precise representation of emissions in the target grids.

Proxy data uncertainty analysis

The construction of gridded CO_2 emission inventory involved an estimation process based on proxy data, and it was, therefore, key to analyzing the proxy data uncertainty. The uncertainty typically stemmed from spatial uncertainty, insufficient representativeness, or lack of proxy data[50]. The characterization of the proxy data uncertainty in gridded inventories focused on two aspects, i.e., the proxy data uncertainty of point source emissions and non-point source emissions. In this study, it was assumed that these two types of uncertainty were independent of each other and could be aggregated by the error transfer algorithm to summarize the overall proxy data uncertainty. This study conducted uncertainty estimation and analysis for the four highest-emission sectors, including two point source sectors, industrial energy and industrial processing, and two non-point source sectors, transportation and residents.

For point source emissions, the proxy data uncertainty could be set to 0 because of the manual geographic identification of high-emission point source emissions one by one in this study. The proxy data uncertainty of non-point source emissions was mainly concentrated in residential emissions and transportation emissions. The proxy data uncertainty of transportation emissions was determined by the drift value of traffic volume, which was set to ±5% of road traffic volume. For the latter, we estimated by the grid drift method[51]. The target grid was moved by 10% of the grid length in the direction of south, north, east, and west, resulting in four drifted grids. Subsequently, we calculated the weighted sum by applying a ratio of 90% of the target grid's population and 10% of the adjacent grid's population in each drifted grid. This process yielded the weighted population data for the four drifted girds, from which the standard deviation of population data was computed as the proxy data uncertainty for the target grid.

After separately calculating the proxy data uncertainties of point and non-point sources, the uncertainties of the above emissions were aggregated by using the error transfer algorithm, resulting in the proxy data uncertainty of inventory.

RESULTS

Gridded CO_2 emission inventory and results analysis

The spatial allocation results of the CO_2 emission inventory for 2020 in Chengdu, namely the high-resolution emission inventory of Chengdu (HEI-CD), are shown in Figure 5A. This figure illustrates the spatial distribution of emission intensity within the study area. Different colored grids represent varying levels of emission intensity, measured in tons per square kilometer per year ($t \cdot km^{-2} \cdot yr^{-1}$). Red areas indicate the highest emission intensity, while blue areas indicate the lowest.

In the study area, three high-emission areas are identified [Figure 5B]: the city center, the northwest industrial zone, and the eastern power plant region. The combined emissions from these three high-emission areas total 20,228 kt, accounting for 52.9% of the total emissions of Chengdu. Region 1, which represents emission intensity in the city center, includes five districts: Qingyang District, Wuhou District, Jinniu District, Chenghua District, and Jinjiang District. Emissions in this area total 8,238 kt, with an emission intensity of 5.51 $kt \cdot km^{-2} \cdot yr^{-1}$. This region has a dense population, a well-developed road network, and numerous service facilities, with emissions primarily from transportation and residents. Region 2, located in the northwest industrial zone, mainly includes Dujiangyan City and Pengzhou. City. The emissions for this region amount to 8,164 kt, with an emission intensity of 9.21 $kt \cdot km^{-2} \cdot yr^{-1}$, accounting for approximately 21.3% of the total emissions. This area contains a large number of chemical enterprises and several building materials enterprises, with cement manufacturing plants being the primary source of CO_2 emissions. The cement manufacturing process requires the combustion of large amounts of coal to calcine limestone. Coal combustion produces significant amounts of CO_2, and the thermal decomposition of limestone also generates substantial CO_2 emissions. The cement industry has become a major global source of CO_2 emissions, with fuel combustion accounting for 35% and the calcination process for approximately 52%[52]. Region 3 is situated on the eastern side of the city center, within the territory of Jintang County. The total emissions for this region amount to 3,827 kt, accounting for 10%. The primary source of these emissions is fossil fuel combustion at a major power plant.

Chengdu currently comprises 20 district- and county-level administrative units, along with 371 township- and subdistrict-level administrative units. The emission intensity and quantity for each district, county, county-level city, township, town, and subdistrict are shown in Figure 5C, with the emission quantity of town-level administrative units represented by a color bar and the emission intensity of district-level units depicted by histograms. The top five districts with the highest emission intensities are located in the city

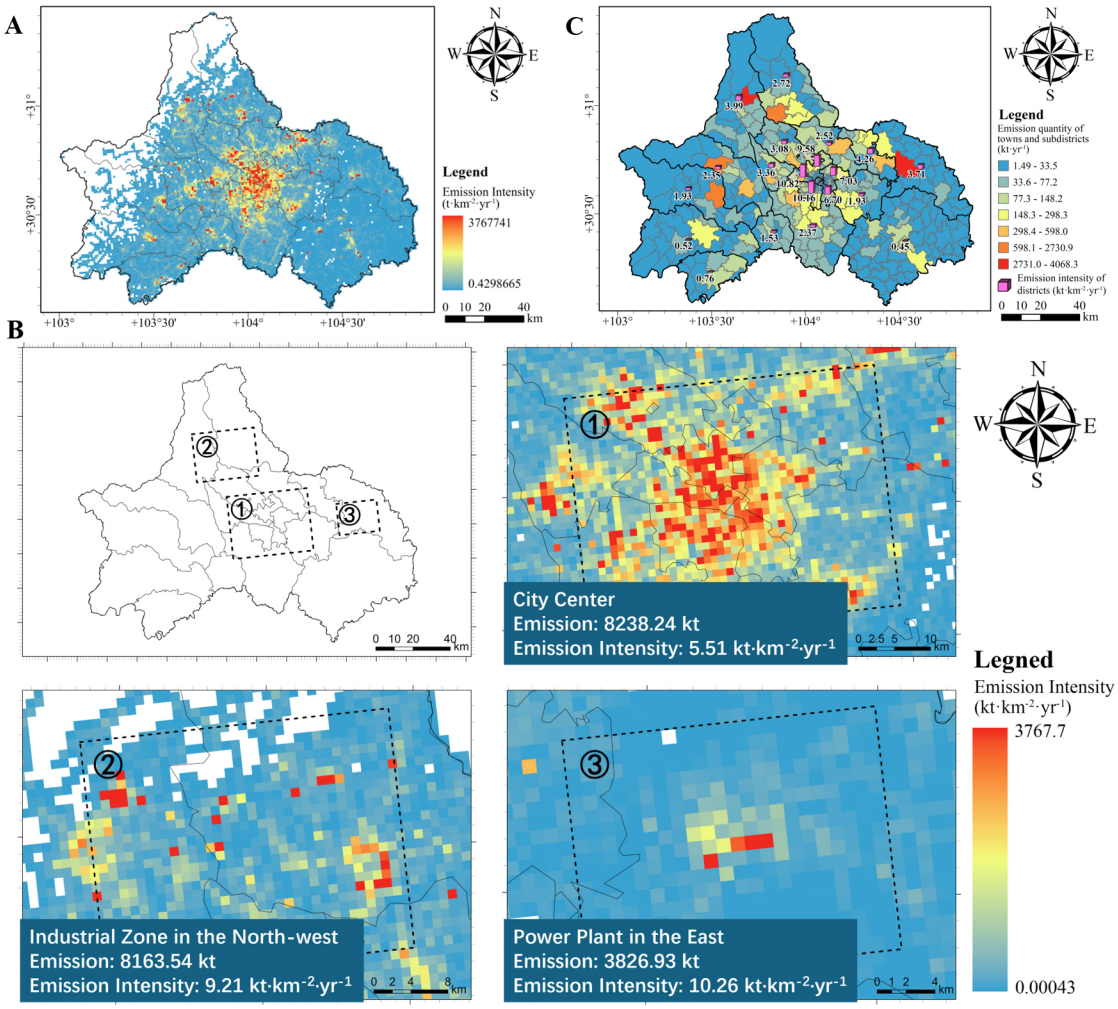

Figure 5. Gridded CO_2 emission inventory compilation results and analysis: (A) Gridded CO_2 emission for Chengdu in 2020; (B) Spatial distribution and local enlargement of high-emission areas; (C) Emission quantity of town-level administrative units and emission intensity of district-level administrative units.

center: Qingyang District, Wuhou District, Jinniu District, Chenghua District, and Jinjiang District. Their emission intensities, ranked from highest to lowest, all exceed 5 kt·km^{-2}·yr^{-1}. Specifically, Qingyang District has the highest intensity at 10.82 kt·km^{-2}·yr^{-1}, followed by Wuhou District at 10.16 kt·km^{-2}·yr^{-1}. In contrast, the three districts with the lowest emission intensities are Pujiang County (0.76 kt·km^{-2}·yr^{-1}), Qionglai City (0.52 kt·km^{-2}·yr^{-1}), and Jianyang City (0.45 kt·km^{-2}·yr^{-1}), all recording values below 1 kt·km^{2}·yr^{-1}. From the spatial distribution perspective, it is obvious that emission intensity increases closer to the city center and decreases with far distance. Furthermore, emissions in the southern region are notably lower compared to those in the northern region. Based on the emission quantity analysis, the emission levels in the five city central districts are significantly lower than those in the surrounding areas. In particular, Jinjiang District has the lowest emissions among the 20 districts, totaling only 406.5 kt·yr^{-1}. Conversely, Dujiangyan City exhibits the highest emissions at 4,832.6 kt·yr^{-1}, followed by Jintang County with emissions totaling 4,281.3 kt·yr^{-1}. Importantly, these two areas are also where the aforementioned high-emission point sources are located. This demonstrates that the high-emission point source distribution, particularly cement manufacturing plants and thermal power plants, determines whether an administrative area is characterized by high emissions. Factors such as population and road network density influence emission intensity,

particularly in the city center. Despite lower total emissions, the city center exhibits higher emission intensity, indicating a larger number of emissions per unit area.

Spatial distribution characteristics of CO_2 emissions by sector

The spatial distribution characteristics of emissions from various sectors are presented in Figure 6. Figure 6A-C depict the spatial distribution of point source emissions for industrial energy emissions, industrial processing emissions, and service emissions, respectively. Due to the high density of point sources in industrial energy and service emissions, these were subjected to gridding. The industrial energy emissions comprise a total of 5,335 point source emissions. High-emission point sources are primarily concentrated in the areas surrounding the city center. Shuangliu District has the highest number of point sources, totaling 646, followed by Pidu District with 598 and the adjacent Xindu District with 538. Analysis of industrial energy emissions by district reveals that Jintang County, home to a power plant, has the highest emissions at 3,727 $kt \cdot yr^{-1}$. In contrast, Shuangliu District, despite having the largest number of point sources, has emissions of only 627 $kt \cdot yr^{-1}$, ranking seventh. This indicates that the key determinant of regional industrial energy emissions is not the number of emitting enterprises but the industrial structure of this region. In contrast to industrial energy emissions, the number of point sources for industrial processing emissions is significantly lower. There are five point sources from the cement production process, two from the limestone production process, and four from the steel production process. The cement production process is the largest contributor to emissions of this type. The top three emitters collectively contributed the majority of emissions, with a total of 6,831 $kt \cdot yr^{-1}$. The emissions from the limestone production process are similar to those from the cement production process. However, due to the lower production volume of limestone compared to cement, the emissions are significantly lower than that of cement. Service emissions are more widely distributed, primarily concentrated in the city center and the central areas of the various subordinate cities and counties. The total number of service point sources is approximately 66,000.

The spatial distribution characteristics of non-point source emissions, which are indicated in Figure 6D, Figure 4E and F, mainly arise from residents, agriculture, and transportation emissions. The spatial distribution of residents' emissions [Figure 6D] is entirely dependent on the population distribution. High-emission areas are concentrated in the city center, with the highest emission intensity reaching 8,655 $kt \cdot km^{-2} \cdot yr^{-1}$. Agriculture emissions [Figure 6E] are predominantly found in the plain areas on the outskirts of the urban, mainly on the southern and eastern sides. The western region, affected by the Qinghai-Tibet Plateau, is mostly mountainous terrain and unsuitable for agricultural cultivation, thus resulting in virtually no agriculture emissions. Transportation emissions [Figure 6F], as a major non-point source, are widely distributed, with the highest emission intensity reaching 13,964 $kt \cdot km^{-2} \cdot yr^{-1}$. They are influenced by road network density and traffic volume. Highways have high traffic volume but lower road network density, resulting in lower emission intensity compared to secondary roads with higher road network density in the city center. The distribution characteristics conform to the pattern of high emission intensity in the city center, radiating outward.

Estimation and analysis of proxy data uncertainty

Due to the lack of uncertainty estimation in the tabular inventory provided by CCCED, this study only addressed uncertainties resulting from proxy data deficiencies. The primary focus focused on the uncertainties associated with four major emission sectors: industrial energy, industrial processing, transportation, and residents. For the first two sectors, the locations of high-emission point sources were manually verified, ensuring the location information was absolutely accurate and resulting in the uncertainty of 0 for industrial energy and industrial processing proxy data.

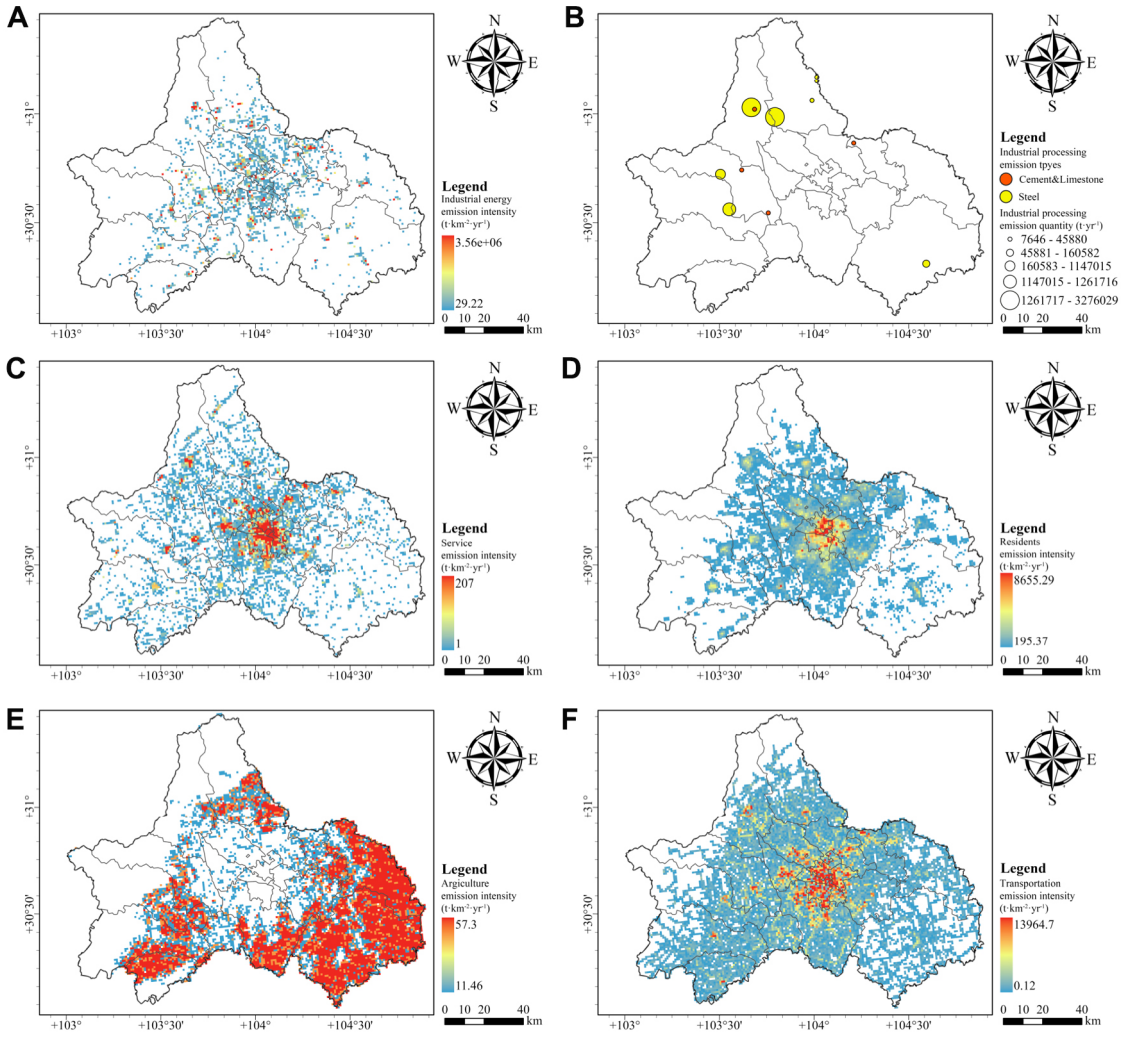

Figure 6. Spatial allocation of emissions by each sector: (A) Industrial energy emission; (B) Industrial processing emission; (C) Service emission; (D) Residents emission; (E) Agriculture emission; (F) Transportation emission.

The uncertainties for the two main non-point source emissions were estimated using the method described in previous sections. They were aggregated to obtain absolute [Figure 7A] and relative [Figure 7B] proxy data uncertainties. The analysis revealed a strong correlation between the spatial distribution of absolute uncertainty and emissions, with higher uncertainty in high-emission areas and lower uncertainties in low-emission areas. The highest uncertainty recorded was 712 t. The relative uncertainty distribution indicated lower values in the city center and higher values in suburban areas. Overall, the uncertainty across the study area was relatively low and fell within acceptable limits.

Comparison results and analysis of gridded emission inventories

The processed HEI-CD model was compared and analyzed against the widely used EDGAR inventory, which was commonly applied in city-scale CO_2 emission inversion. Due to the substantial variance in spatial resolution between the two inventories, with the HEI-CD model operating at a resolution of 1 km and EDGAR inventory at 0.1° (approximately 9.6 km at Chengdu's latitude), direct overlay comparison was unfeasible. To facilitate comparison, the HEI-CD model would be upscaled and resampled onto grids with a resolution of 0.1°, aligning with the spatial resolution of the EDGAR inventory. This process would yield a

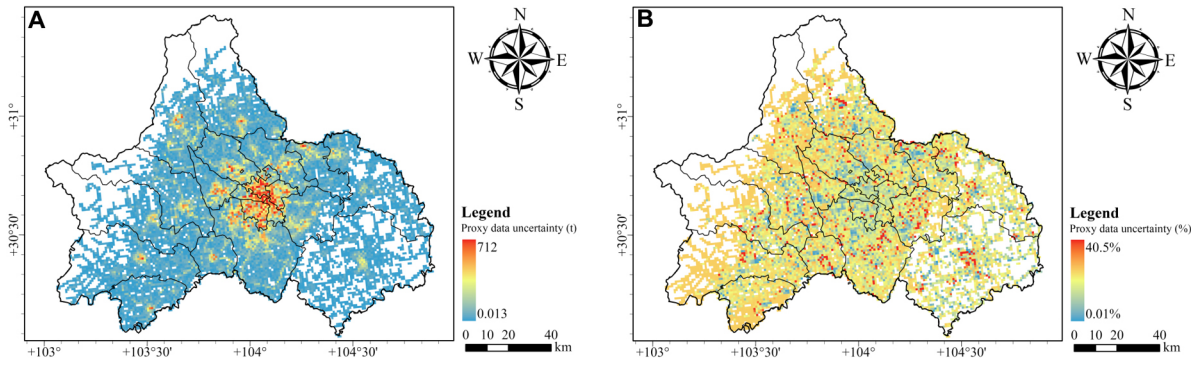

Figure 7. Spatial distribution characteristics of absolute (A) and relative (B) Uncertainties in proxy data.

HEI-CD model with a 0.1° resolution [Figure 8A], enabling a valid comparison with the EDGAR inventory [Figure 8B]. To compare the two inventories, the difference is shown in Figure 8C, where red areas indicate higher emissions in the HEI-CD model and blue areas indicate higher emissions in the EDGAR inventory.

The spatial distribution of the HEI-CD model was broadly similar to that of the EDGAR inventory. Both inventories exhibited a spatial distribution pattern where emissions were generally higher in the city center than in the surrounding areas. However, the surrounding areas showed several high-emission point sources. Both accurately characterized the high-emission characteristics of key cement production facilities. However, the HEI-CD model slightly underestimated emissions in this area compared to the EDGAR inventory, likely due to the more comprehensive point source information in the HEI-CD model, resulting in a lower allocation of emissions to this region.

In the western side of the study area, the HEI-CD model identified two high-emission areas, indicating that the EDGAR inventory lacked accurate point source data for this region, thus failing to accurately represent emissions here. Conversely, on the southern side, the EDGAR inventory overestimated emissions. Visual inspection did not identify potential high-emission sources, suggesting a likely overestimation by EDGAR in this area. In the area of High-Emission Zone 3, located in the eastern part of the study region, EDGAR inventory incorrectly represented the location of the power plant, resulting in discrepancies in high-emission areas. In the city center, the EDGAR inventory also slightly overestimated emissions compared to the HEI-CD model.

A histogram [Figure 8D] was generated through quantitative statistical analysis of the differences between the HEI-CD model and the EDGAR inventory. The histogram revealed that the majority of the emission differences were centered around the median value of -7.04 kt, with the highest count reaching 120. This suggested that most points exhibited a small negative emission difference, indicating that the emission intensities were closely aligned in most areas. It also implied that the HEI-CD model generally estimated slightly lower emissions than the EDGAR inventory.

DISCUSSION

Interpretation of study results

This study successfully developed a high-resolution, city-scale gridded CO_2 emission inventory for Chengdu, providing a detailed spatial distribution of emissions across various sectors. The analysis identified three primary high-emission areas: the densely populated city center, the industrially active northwest region, and the energy-intensive eastern area. Together, these regions accounted for over 40% of

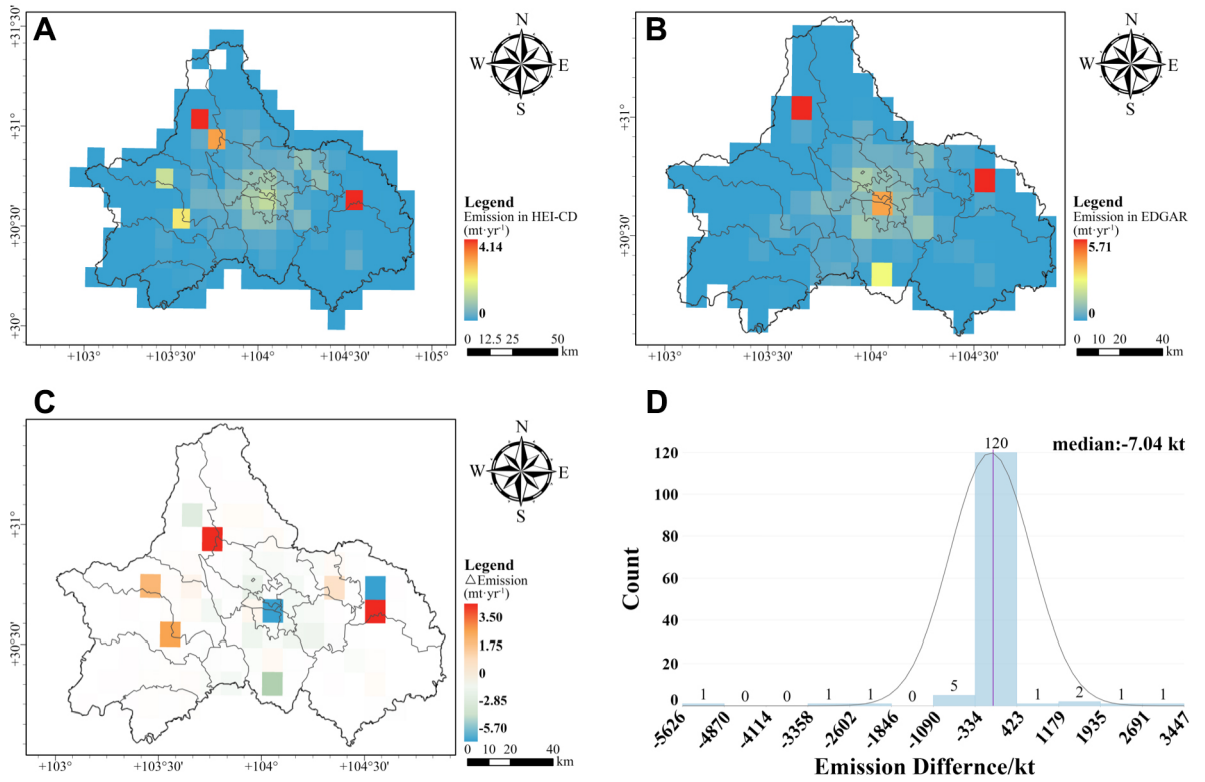

Figure 8. Comparison and results between HEI-CD model and EDGAR inventory: (A) Regirded HEI-CD model with 0.1° spatial resolution; (B) EDGAR inventory for study area; (C) Difference HEI-CD model and EDGAR inventory; (D) Frequency histogram of difference for each grid.

total CO_2 emissions, with significant contributions from industrial processing, transportation and power production.

The finding highlighted the importance of incorporating high resolution in emission inventories, particularly in city environments where emission sources are concentrated and diverse. By integrating multiple open data sources and employing a spatial allocation algorithm, this study offered an accurate and reliable prior inventory for CO_2 emission flux inversion in urban carbon monitoring, laying the groundwork for effective policy interventions.

Policy implications and urban carbon reduction strategies

This study offered a valuable tool for policymakers aiming to address urban carbon emissions at a detailed level. The high-resolution gridded CO_2 emission inventory for Chengdu reveals specific high-emission zones, particularly in industrial and densely populated city areas. Such spatial precision allowed for more targeted policy interventions, which were essential for effective carbon reduction in rapidly urbanized cities including Chengdu. Unlike traditional broad-based policies that lack spatial specificity, the results suggested that local management, such as enhancing energy efficiency in industrial sectors and improving urban transport infrastructure, could significantly contribute to the carbon reduction goals. It was necessary for Chengdu and similar cities to adopt a multifaceted approach to carbon reduction, considering both regulatory measures and incentives for the adoption of green technologies. This approach included stricter emissions standards, subsidies for clean energy technologies, and investments in public transportation infrastructure. Moreover, this study underscored the importance of continuously monitoring and updating

emission inventories to keep pace with the dynamic changes in city development and industrial activities, while also ensuring that future developments align with the long-term sustainability objectives.

Comparison with EDGAR inventory

The comparison between the HEI-CD model and the widely used EDGAR inventory revealed both the strengths and limitations of each approach. The EDGAR inventory, with its global coverage and long-term data records, was invaluable for large-scale atmospheric modeling and international climate assessments, making it particularly suitable for CO_2 emission flux inversions at global or national levels. However, its relatively low spatial resolution (0.1° × 0.1°) limited the applicability for city-scale or high-resolution inversions, where detailed spatial information was crucial for accurately mapping emissions and informing policy decisions.

In contrast, the HEI-CD model offered a much higher spatial resolution (1 km × 1 km), which was better suited for small-scale inversions, especially at the city scale. The improved accuracy in point source information, as provided by the HEI-CD model, significantly enhanced the quality of inversion by more precisely capturing the spatial variability of emissions. This high resolution enabled more accurate identification of emission hotspots and a more detailed understanding of the spatial distribution of emissions within the city, ultimately leading to reliable results in atmospheric modeling.

However, the higher resolution in the HEI-CD model requires detailed and often harder-to-obtain data, and the reliance on proxy data can introduce uncertainties due to variations in data choice, quality and availability. Nevertheless, for urban carbon monitoring and management, the HEI-CD model represents a substantial improvement over broader-scale inventories like EDGAR, offering a tailored approach to local emission reduction efforts.

Improvement relative to previous studies

This study achieved high-resolution gridded CO_2 emission inventories by integrating multiple open data sources for spatial proxies. Unlike previous studies that relied on relatively homogeneous proxy data (e.g., nighttime lights[40] or NDVI[53]), this study used diverse, sector-specific, high-resolution proxy data, including population distribution, road networks, and industrial point sources, to describe city CO_2 emissions with greater detail and accuracy.

Compared to global-scale inventories like EDGAR which was suited for broader scales, this inventory at the city scale provided a detailed view of city emissions, improving hotspot identification, enhancing the ability of CO_2 emission flux inversion, and supporting better-informed policy decisions. Similarly, previous studies, like the Vulcan inventory by Gurney *et al.* (2009)[54] and vehicle emission inventory by Cai *et al.* (2020)[55] and Sun *et al.* (2021)[36], either focus on specific sectors or lack the comprehensive integration of sector-specific data that our study achieves. The sector-specific spatial allocation strategy employed here reduces uncertainties by tailoring methods to the unique characteristics of each sector, providing a more accurate foundation for CO_2 monitoring and mitigation efforts.

Study limitations and future directions

Despite the advancements presented in this study, several limitations warrant discussion. First, the reliance on proxy data for non-point sources, such as residents and agriculture emissions, introduces uncertainty into the inventory. While efforts have been made to minimize uncertainties through careful data selection and processing, the inherent variability in proxy data quality remains challenging. Future research should explore the integration of high-resolution and representative data sources, such as smart city infrastructure data or detailed land-use records based on remote sensing technologies, to further refine the accuracy of emission inventories.

Another limitation was the exclusion of certain low-emission sources, such as aviation and some industries, due to data availability constraints. This omission means that the inventory may not fully capture all city emissions, potentially leading to an underestimation of the total carbon footprint. To address this, future studies should aim to include a broader range of emission sources by leveraging new data collection methods or collaborating with industry stakeholders to gain access to proprietary data.

Moreover, the emission allocation for individual point sources was based on weight data such as a company's registered or paid-in capital. While this approach allowed for the distribution of emission data, it introduced uncertainty regarding the actual emissions from each point source. This method could not accurately reflect the specific operational details of each company, thus reducing the precision of point source emissions in the inventory. Although this study achieved better point source identification than large-scale inventories, there were still cases where companies were missing from the API interface of the online map platform. In future work, it will be necessary to cross-check results from online map platforms with enterprise information enquiry systems to minimize the omission of point sources and improve the completeness of the inventory.

Looking forward, there is a clear need for the development of validating systems and automated methods for updating the inventory. The dynamic nature of city environments, characterized by ongoing industrial activities, transportation network changes, and population shifts, necessitates the ability to frequently update emission inventories. Automation could involve the use of machine learning algorithms to continuously refine spatial allocation models or the deployment of sensor networks to provide real-time emission data.

In addition to automation, the validation systems of the emission inventory should become a focal point in future work. This involves using the compiled gridded emission inventory as a prior inventory in atmospheric transport models to simulate CO_2 concentrations. By combining simulated concentrations with observed concentrations, a posterior inventory that better reflects actual emission distributions can be inversed through a Bayesian inversion framework. Such comparisons will allow for the identification of biases and discrepancies in the prior inventory, leading to accurate and optimized emission estimates. This continuous loop of validation and optimization is critical for maintaining the relevance and accuracy of inventories, ensuring that it effectively supports urban carbon reduction policies.

These advancements, both in automation and validation, will be crucial in enhancing the utility of the inventory in cities like Chengdu toward their carbon neutrality goals. As city environments continue to evolve, the ability to dynamically update and validate emission inventories will be essential for effective carbon management.

CONCLUSION

This study developed a detailed gridded CO_2 emission inventory for Chengdu, which is tailored for city-scale CO_2 emission flux inversions. By integrating multiple open data sources and employing a spatial allocation algorithm, the inventory provided a detailed and accurate spatial description of CO_2 emissions across various sectors. The analysis identified key high-emission areas, particularly in the densely populated city center, the industrially active northwest region, and the energy-intensive eastern area, collectively accounting for a significant portion of total emissions.

Compared to the EDGAR inventory, the HEI-CD model offered greater spatial resolution and precise point source information, which was better suited for urban carbon monitoring and policy-making at the city scale. The inventory will not only support the accurate inversion of CO_2 emission flux but also serve as a crucial tool for guiding effective carbon reduction strategies.

Future work should focus on further refining the inventory through the introduction of additional data sources, enhancing validation systems, and ensuring adaptability to the dynamic nature of city environments. This will solidify its role in supporting Chengdu and similar cities in their efforts toward carbon neutrality.

DECLARATIONS

Authors' contributions

Made substantial contributions to the conception and design of the study and performed data analysis and interpretation: Wang R

Performed data acquisition, as well as providing administrative, technical, and material support: Zhang Y, Zhao S, Wang X

Availability of data and materials

The data presented in this work are available upon reasonable request from the corresponding author.

Financial support and sponsorship

This work was supported by the National Key Research and Development Program of China (2022YFE0209100), the National Natural Science Foundation of China (42307129), and the Zhejiang Provincial Natural Science Foundation (LZJMZ24D050005).

Conflicts of interest

All authors declared that there are no conflicts of interest.

Ethical approval and consent to participate

Not applicable.

Consent for publication

Not applicable.

REFERENCES

1. Filonchyk M, Peterson MP, Zhang L, Hurynovich V, He Y. Greenhouse gases emissions and global climate change: examining the influence of CO_2, CH_4, and N_2O. *Sci Total Environ* 2024;935:173359. DOI PubMed
2. Rogelj J, den Elzen M, Höhne N, et al. Paris agreement climate proposals need a boost to keep warming well below 2 °C. *Nature* 2016;534:631-9. DOI
3. Ward DS, Mahowald NM. Contributions of developed and developing countries to global climate forcing and surface temperature change. *Environ Res Lett* 2014;9:074008. DOI
4. Wei T, Yang S, Moore JC, et al. Developed and developing world responsibilities for historical climate change and CO_2 mitigation. *Proc Natl Acad Sci USA* 2012;109:12911-5. DOI PubMed PMC
5. Shafique M, Azam A, Rafiq M, Luo X. Life cycle assessment of electric vehicles and internal combustion engine vehicles: a case study of Hong Kong. *Res Transp Econ* 2022;91:101112. DOI
6. Bui M, Adjiman CS, Bardow A, et al. Carbon capture and storage (CCS): the way forward. *Energy Environ Sci* 2018;11:1062-176. DOI

7. Wang Y, Guo CH, Chen XJ, et al. Carbon peak and carbon neutrality in China: goals, implementation path and prospects. *China Geol* 2021;4:720-46. DOI
8. Xi JP. Building on past achievements and launching a new journey for global climate actions. 2020. DOI
9. Cai B, Lu J, Wang J, et al. A benchmark city-level carbon dioxide emission inventory for China in 2005. *Appl Energy* 2019;233-4:659-73. DOI
10. Reckien D, Flacke J, Dawson RJ, et al. Climate change response in Europe: what's the reality? Analysis of adaptation and mitigation plans from 200 urban areas in 11 countries. *Clim Chang* 2014;122:331-40. DOI
11. Heidrich O, Dawson RJ, Reckien D, Walsh CL. Assessment of the climate preparedness of 30 urban areas in the UK. *Clim Chang* 2013;120:771-84. DOI
12. Yang X, Wang XC, Zhou ZY. Development path of Chinese low-carbon cities based on index evaluation. *Adv Clim Chang Res* 2018;9:144-53. DOI
13. Wang WZ, Liu LC, Liao H, Wei YM. Impacts of urbanization on carbon emissions: an empirical analysis from OECD countries. *Energy Policy* 2021;151:112171. DOI
14. Wei T, Wu J, Chen S. Keeping track of greenhouse gas emission reduction progress and targets in 167 cities worldwide. *Front Sustain Cities* 2021;3:696381. DOI
15. Rosenzweig C, Solecki W, Hammer SA, Mehrotra S. Cities lead the way in climate-change action. *Nature* 2010;467:909-11. DOI PubMed
16. Dhakal S. Urban energy use and carbon emissions from cities in China and policy implications. *Energy Policy* 2009;37:4208-19. DOI
17. Zhu XH, Lu KF, Peng ZR, He HD, Xu SQ. Spatiotemporal variations of carbon dioxide (CO_2) at urban neighborhood scale: characterization of distribution patterns and contributions of emission sources. *Sustain Cities Soc* 2022;78:103646. DOI
18. Zhang M, Tan S, Zhang C, Chen E. Machine learning in modelling the urban thermal field variance index and assessing the impacts of urban land expansion on seasonal thermal environment. *Sustain Cities Soc* 2024;106:105345. DOI
19. Wang R, Gao W, Zhou N, Kammen DM, Peng W. Urban structure and its implication of heat stress by using remote sensing and simulation tool. *Sustain Cities Soc* 2021;65:102632. DOI
20. Zhang M, Zhang Z, Tong B, Ren B, Zhang L, Lin X. Analysis of the coupling characteristics of land transfer and carbon emissions and its influencing factors: a case study of China. *Front Environ Sci* 2023;10:1105552. DOI
21. Fang G, Gao Z, Tian L, Fu M. What drives urban carbon emission efficiency? - Spatial analysis based on nighttime light data. *Appl Energy* 2022;312:118772. DOI
22. Xu J, Wang J, Li R, Yang X. Spatio-temporal effects of urbanization on CO_2 emissions: evidences from 268 Chinese cities. *Energy Policy* 2023;177:113569. DOI
23. He X, Guan D, Yang X, Zhou L, Gao W. Quantifying the trends and affecting factors of CO_2 emissions under different urban development patterns: an econometric study on the Yangtze river economic belt in China. *Sustain Cities Soc* 2024;107:105443. DOI
24. Huang Y, Ou J, Deng Z, Zhou W, Liang Y, Huang X. Peak patterns and drivers of city-level daily CO_2 emissions in China. *J Clean Prod* 2024;469:143206. DOI
25. Scarpelli TR, Jacob DJ, Grossman S, et al. Updated global fuel exploitation inventory (GFEI) for methane emissions from the oil, gas, and coal sectors: evaluation with inversions of atmospheric methane observations. *Atmos Chem Phys* 2022;22:3235-49. DOI
26. Crippa M, Guizzardi D, Schaaf E, et al; Joint Research Centre (European Commission). GHG emissions of all world countries. Publications Office of the European Union; 2023. DOI
27. Janssens-Maenhout G, Crippa M, Guizzardi D, et al. EDGAR v4.3.2 global atlas of the three major greenhouse gas emissions for the period 1970-2012. *Earth Syst Sci Data* 2019;11:959-1002. DOI
28. Crippa M, Solazzo E, Huang G, et al. High resolution temporal profiles in the emissions database for global atmospheric research. *Sci Data* 2020;7:121. DOI PubMed PMC
29. Scarpelli TR, Jacob DJ, Octaviano Villasana CA, et al. A gridded inventory of anthropogenic methane emissions from Mexico based on Mexico's national inventory of greenhouse gases and compounds. *Environ Res Lett* 2020;15:105015. DOI
30. Hu C, Griffis TJ, Xia L, et al. Anthropogenic CO_2 emission reduction during the COVID-19 pandemic in Nanchang City, China. *Environ Pollut* 2022;309:119767. DOI PubMed PMC
31. Maasakkers JD, Jacob DJ, Sulprizio MP, et al. Global distribution of methane emissions, emission trends, and OH concentrations and trends inferred from an inversion of GOSAT satellite data for 2010-2015. *Atmos Chem Phys* 2019;19:7859-81. DOI
32. Lyon DR, Zavala-Araiza D, Alvarez RA, et al. Constructing a spatially resolved methane emission inventory for the barnett shale region. *Environ Sci Technol* 2015;49:8147-57. DOI
33. Lauvaux T, Miles NL, Deng A, et al. High-resolution atmospheric inversion of urban CO_2 emissions during the dormant season of the Indianapolis Flux Experiment (INFLUX). *J Geophys Res Atmos* 2016;121:5213-36. DOI PubMed PMC
34. Turner AJ, Shusterman AA, Mcdonald BC, Teige V, Harley RA, Cohen RC. Network design for quantifying urban CO_2 emissions: assessing trade-offs between precision and network density. *Atmos Chem Phys* 2016;16:13465-75. DOI
35. Xu YQ, Luo YL, Fu GY, et al. Status of developing high-precision greenhouse gas emission inventory in China. *Environ Monit China* 2023;39:52-9. DOI
36. Sun S, Sun L, Liu G, et al. Developing a vehicle emission inventory with high temporal-spatial resolution in Tianjin, China. *Sci Total Environ* 2021;776:145873. DOI
37. Li Y, Lv C, Yang N, Liu H, Liu Z. A study of high temporal-spatial resolution greenhouse gas emissions inventory for on-road

vehicles based on traffic speed-flow model: a case of Beijing. *J Clean Prod* 2020;277:122419. DOI

38. Azhari A, Abdul Halim ND, Othman M, et al. Highly spatially resolved emission inventory of selected air pollutants in Kuala Lumpur's urban environment. *Atmosp Pollut Res* 2021;12:12-22. DOI
39. Sun C, Wang B, Miao H. Spatiotemporal dynamics of CO_2 emissions: a case study of the "New Yangtze River Delta" in China. *Environ Sci Pollut Res Int* 2023;30:40961-77. DOI
40. Cui X, Lei Y, Zhang F, Zhang X, Wu F. Mapping spatiotemporal variations of CO_2 (carbon dioxide) emissions using nighttime light data in Guangdong province. *Phys Chem Earth Parts A/B/C* 2019;110:89-98. DOI
41. China City Greenhouse Gas Working Group. China city carbon dioxide emission dataset. 2020. Available from: https://www.cityghg.com/toArticleDetail;jsessionid=52C5671AF69E4CB1E74D601EB4BAD486?id=203 [Last accessed on 19 Sep 2024].
42. Tianyancha. Available from: https://www.tianyancha.com/ [Last accessed on 19 Sep 2024].
43. Bondarenko M, Kerr D, Sorichetta A, Tatem AJ. Census/projection-disaggregated gridded population datasets, adjusted to match the corresponding UNPD 2020 estimates, for 183 countries in 2020 using Built-Settlement Growth Model (BSGM) outputs. University of Southampton, UK: WorldPop; 2020. DOI
44. Earth Observation Group. See the world at night. Available from: https://eogdata.mines.edu/products/vnl/ [Last accessed on 19 Sep 2024].
45. Foundation O. OpenStreetMap data extracts. Available from: https://download.geofabrik.de/ [Last accessed on 19 Sep 2024].
46. China MoHaU-RDotPsRo. Code for design of urban road engineering. Beijing: China Architecture & Building Press; 2012. pp.8-9.
47. China MoTotPsRo. Technical standard of highway engineering. Beijing: China Communication Press; 2003. pp.1-9.
48. MarineTraffic. Automatic identification system. Available from: https://www.marinetraffic.com/ [Last accessed on 21 June 2024].
49. Damien SM, Mark F. MCD12Q1 v061 - MODIS/Terra+Aqua land cover type yearly L3 global 500 m SIN grid. Available from: https://lpdaac.usgs.gov/products/mcd12q1v061/ [Last accessed on 19 Sep 2024].
50. He J, Wang Z, Zhao L, et al. Gridded emission inventory of organophosphorus flame retardants in China and inventory validation. *Environ Pollut* 2021;290:118071. DOI
51. Hogue S, Marland E, Andres RJ, Marland G, Woodard D. Uncertainty in gridded CO_2 emissions estimates. *Earth's Future* 2016;4:225-39. DOI
52. Czigler T, Reiter S, Schulze P, Somers K. Laying the foundation for zero-carbon cement. McKinsey & Company; 2020. Available from: https://www.mckinsey.com/industries/chemicals/our-insights/laying-the-foundation-for-zero-carbon-cement [Last accessed on 19 Sep 2024]
53. Xu Q, Dong YX, Yang R, Zhang HO, Wang CJ, Du ZW. Temporal and spatial differences in carbon emissions in the Pearl River Delta based on multi-resolution emission inventory modeling. *J Clean Prod* 2019;214:615-22. DOI
54. Gurney KR, Mendoza DL, Zhou Y, et al. High resolution fossil fuel combustion CO_2 emission fluxes for the united states. *Environ Sci Technol* 2009;43:5535-41. DOI
55. Cai M, Shi Y, Ren C. Developing a high-resolution emission inventory tool for low-carbon city management using hybrid method - a pilot test in high-density Hong Kong. *Energy Build* 2020;226:110376. DOI